Thin Solid Films 736 (2021) 138909

Contents lists available at ScienceDirect

Thin Solid Films

journal homepage: www.elsevier.com/locate/tsf

Applying surface-sensitive techniques to structural and chemical study of uncapped Sn-Sb-Te thin film. A density functional theory - based study

V. Bilovol [a,b,*], H.H. Medina Chanduví [c], L.A. Errico [c,d,e]

[a] Universidad de Buenos Aires, Facultad de Ingeniería, Laboratorio de Sólidos Amorfos, Av. Paseo Colón 850, C1063ACV, Buenos Aires, Argentina
[b] CONICET, Universidad de Buenos Aires, Instituto de Tecnologías y Ciencias de la Ingeniería "Hilario Fernández Long" (INTECIN), Av. Paseo Colón 850, C1063ACV, Buenos Aires, Argentina
[c] Departamento de Física, Facultad de Ciencias Exactas, UNLP, 1900 La Plata, Argentina
[d] Instituto de Física La Plata IFLP, CONICET, CCT, La Plata, 1900 La Plata, Argentina
[e] Universidad Nacional Del Noroeste de La Pcia. de Buenos Aires (UNNOBA), Pergamino CP 2700, Buenos Aires, Argentina

ARTICLE INFO

Keywords:
Tin antimony telluride
Thin films
Grazing incidence x-ray diffraction
^{119m}Sn integral conversion electron Möβbauer spectroscopy
Density functional theory
X-ray photoelectron spectroscopy

ABSTRACT

We present here a combined experimental and theoretical study of the structural and chemical properties of polycrystalline Sn-Sb-Te film with nominal composition $SnSb_2Te_4$ grown by pulsed laser deposition technique on mylar substrate. From the experimental side, surface-sensitive techniques as x-ray photoelectron spectroscopy (XPS), grazing incidence x-ray diffractometry (GIXRD) and ^{119m}Sn integral conversion electron Möβbauer spectroscopy (ICEMS) have been applied to the study of the film at room-temperature and under normal conditions of pressure. GIXRD showed that the Sn-Sb-Te film adopted a NaCl- type structure (Fm-3m), and in the detection limits, no other crystalline phase was revealed. ICEMS technique unambiguously indicated the coexistence of two different tin fractions: Sn(II), as expected for the $SnSb_2Te_4$ phase, and Sn(IV), suggesting oxidation of tin. Chemical in-depth profile obtained by means of XPS suggests the oxidation of all the constituent atoms at the topmost layers of the film and the progressive depletion of tin and antimony oxides going depth in the film. The in-depth atomic concentration profiles also reveals a notorious deficiency of Te in the sample. Theoretically, density functional theory-based calculations (assuming that the Sn-Sb-Te film adopts the Fm-3m structure) support the hypothesis that Te - vacancies sites are occupied by oxygen atoms during the natural oxidation process of Sn-Sb-Te film. Additionally, our calculations demonstrated that only the substitution of Te atoms by oxygen ones induces a semiconducting behavior of the otherwise metallic Sn-Sb-Te host.

1. Introduction

Chalcogenide - based materials are versatile systems for many technological applications but, when presented as thin films, such materials are particularly attractive. Phase change- based memories, thermoelectrics, topological insulators, superconductors are some of those potential applications where chalcogenide - based materials have leading positions in terms of fulfillment [1-5]. Therefore, a thorough study of such films at the basic level becomes an important task to have precise control over the material's properties.

Due to its potential application as a base material in phase change memories, $Ge_2Sb_2Te_5$ (GST) composition aroused unprecedented interest in the scientific community [6-8]. It is interesting to notice that this compound, during the amorphous-to-stable crystalline (hexagonal one) transition, exhibits at first a metastable (with cubic lattice) phase in thin films. This cubic version of the $Ge_2Sb_2Te_5$ thin films underlies the fast amorphous-crystalline transition exploited as a principal mechanism in the phase change-based memories.

In the last years, more and more attention is being devoted to another compound of the chalcogenide family, $SnSb_2Te_4$ (SST). This is because, in analogy GST, SST also exhibits a metastable cubic phase when transitioning from amorphous to stable trigonal lattice with attractive transition temperatures [9] besides of other interesting properties.

Recently, cubic $SnSb_2Te_4$ film was investigated as potential 'spin memory' device [10]. Song et al. reported a pressure-induced superconductor phase of SST at extremely low temperature [11]. Sans and co-workers published some important high-pressure findings in trigonal $SnSb_2Te_4$ powdered sample [12]. Also, Wu et al. [13] studied trigonal

* Corresponding author.
E-mail address: vbilovol@fi.uba.ar (V. Bilovol).

https://doi.org/10.1016/j.tsf.2021.138909
Received 2 October 2020; Received in revised form 6 August 2021; Accepted 26 August 2021
Available online 29 August 2021

SST-nanodots (a topological insulator) coupled to doped graphene for high-rate energy storage.

As it is well known, the crystallization temperature is a critical parameter for phase change – based materials. It was reported that the crystallization temperature of GST can be changed by adding an impurity element (O, N, C, etc.) [14-16]. Devices based on such materials can be affected significantly by presence of oxygen improving or worsening their performance. For instance, in the case of GeTe films exposed to air, the crystallization occured at a much lower temperature than the non-exposed ones ($\Delta T = 50°C$), meanwhile for $Ge_2Sb_2Te_5$ films, $\Delta T = 20°C$ [17]. It was found, for instance, in uncapped $Ge_2Sb_2Te_5$ films that Sb and Ge get oxidized [18]. Agati et al. studied Ge - rich GST alloys and found Ge, Sb, Te reduced content in the surface region and oxygen diffuse in almost throughout the entire thickness of 100 nm-film [19]. As far as we know, no similar studies have been reported in the literature up to date regarding $SnSb_2Te_4$ phase.

In order to elucidate the properties of SST films, first of all, the detailed understanding of their chemical composition and structure are of fundamental importance. Moreover, mastering the material becomes a key condition when its best performance requires its synthesis in two dimensions.

In this work the potentiality of three surface-sensitive techniques are gathered in order to follow some aspects of structural and chemical analysis of uncapped Sn-Sb-Te thin film grown by pulsed laser deposition technique and air exposed. A deeper insight of the chemical state and the distribution of the elements in the nominally $SnSb_2Te_4$ film and their in-depth concentration are presented, finding an important presence of oxygen and lacking of Te in the sample. In spite of that the only crystalline (NaCl-type) phase of Sn-Sb-Te phase is witnessed. Additionally, our density functional theory (DFT) - based calculations show that ideal $SnSb_2Te_4$ with cubic lattice is metallic in nature. Only with oxygens substitutionally occupying Te-vacancy sites a semiconductor behaviour is induced. Also, our calculations correctly reproduce the isomer shift associated to Sn(II) in the $SnSb_2Te_4$ structure.

2. Experimental

Sn-Sb-Te ingot was obtained by the melt quenching procedure of a mixture of the elemental components, enclosed in a previously evacuated quartz ampoule and then heated for 8 h at 750°C. The thin film was prepared by laser ablation of the target (fluence ~2.2 J/cm^2), made of ingot pieces, employing a pulsed Nd-YAG laser radiation of $\lambda = 355$ nm and pulses of 5 ns and 10 Hz. The pressure in the chamber during the deposition was as high as about 5×10^{-3} Pa. The substrate used was a commercial mylar film. The target-to-substrate distance used was 6 cm. The estimated thickness of the film was approximately 150 nm. The atomic composition of the Sn-Sb-Te ingot was close to $Sn_{14}Sb_{31}Te_{55}$ [9].

SmartLab Rigaku θ-2θ diffractometer with Cu-Kα radiation was used measuring with 0.05° step and 0.2°/min sweeping velocity. The film was exposed to x-ray radiation using parallel beam set in grazing incidence geometry. Grazing incidence x-ray diffractometry (GIXRD) experiments were carried out keeping the incident angle fixed (ω = 0.3°, 0.7°, 1.0° and 3°).

^{119m}Sn integral conversion electron Möβbauer spectroscopy (ICEMS) was applied to study the film deposited on mylar using the 23.875 keV γ-radiation from a $Ca^{119m}SnO_3$ source of, nominally, 5 mCi. The velocity drive of the spectrometer operated under the constant acceleration mode over 1024 channels. The calibration was carried out employing bcc-Fe as absorber. The measurements were carried out using a conventional ICEMS chamber with a gas mixture of 94% of He and 6% of CH_4. The spectrum was fitted to Lorentzian profiles by least-squares method using the NORMOS 90 program [20].

Thermo Fisher Scientific equipped (model K-Alpha$^+$) with a monocromatic Al K_α source ($h\nu = 1486.68$ eV) and 12 kV voltage was used for x-ray photoelectron spectroscopy (XPS). Survey spectrum is the average of 3 scans per etch, of duration 6 m 45 s each one, step 0.5 eV, pass energy 150 eV. Short scans are the average of 2 ones per etch, of duration 1 m 25 s each one, step 0.05 eV, pass energy 75 eV. The beam spot size was 400 μm. For decapping, Ar$^+$ beam of 500 eV - energy was used. The instrument work function was calibrated using C 1s photoelectron. The binding energies of the core levels were referred to the Fermi level. The XP spectra were analyzed using the Avantage software.

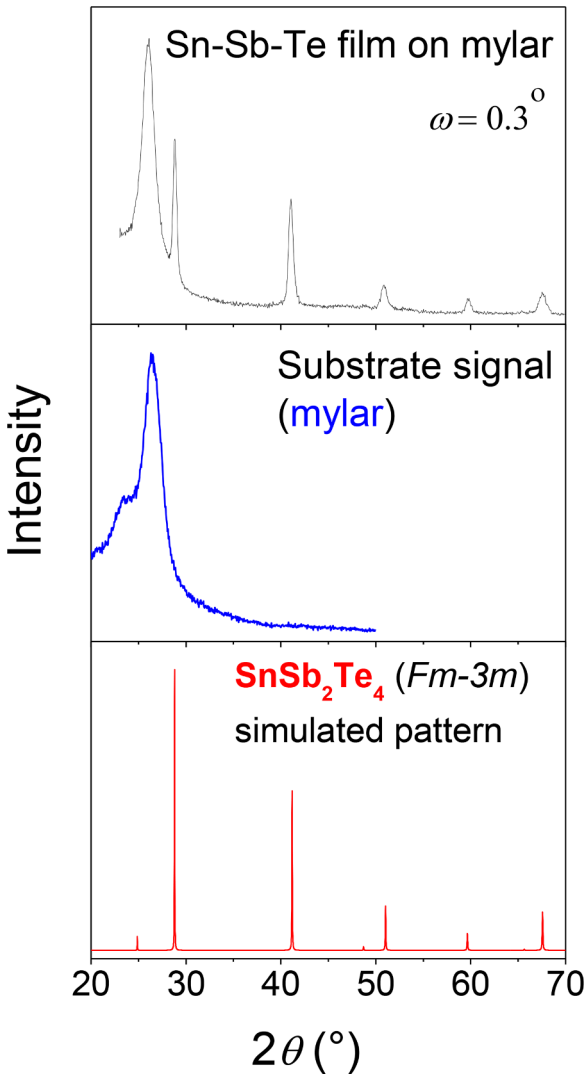

Fig. 1. (top) GIXRD pattern of Sn-Sb-Te film grown on mylar. Incident angle ω = 0.3°; (middle) XRD pattern of mylar; (bottom) simulated XRD pattern of $SnSb_2Te_4$ (space group Fm-3m).

3. Theoretical methodology

The electronic structure calculations were performed using the Wien2K [21] implementation of the full potential linearized augmented plane-wave method [22-24] in a scalar relativistic version. The exchange and correlation (XC) potential were described using the local density approximation (LDA) [25] and different parameterizations of generalized gradient (GGA): Wu-Cohen (WC) - GGA [26], the Perdew-Burke-Ernzenhof (PBE) [27] and PBE-sol [28]. All these approximations for the XC potential yield very similar results. For this reason, we report here the results obtained using WC - GGA. The atomic spheres' radii used for Sn, Te and Sb and O were 1.32 Å and 0.7 Å, respectively. The parameter RK_{max} controls the size of the basis set and was set to 8 for the calculations performed for the case of the unit cell. In the case of the 2ax2ax2a supercell we took $RK_{max} = 7$. Here R is the

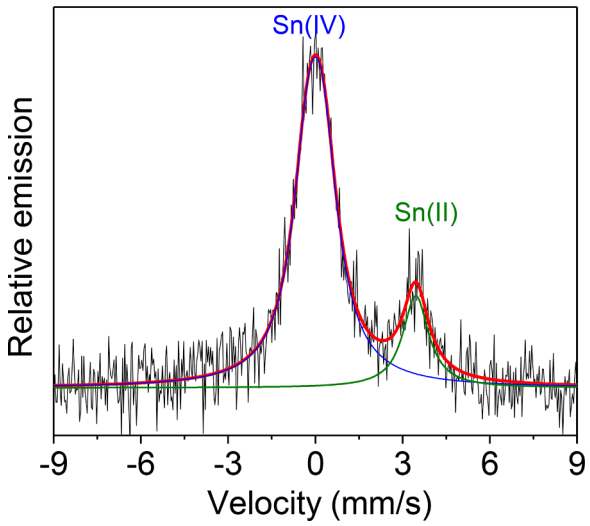

Fig. 2. ICEM spectrum of $SnSb_2Te_4$ film.

smallest muffin-tin radius and K_{max} the largest wave number of the basis set. Atomic internal positions were relaxed until the forces on the atoms were below 0.1 eV/Å. We use this tolerance criterion because a displacement induced by forces smaller than this limit produces changes in the hyperfine parameters that are below the convergence error (see below). Integration in reciprocal space was performed using the tetrahedron method, taking an adequate number of k-points (1000 points for the unit cell, 100 k-points in the case of the 2ax2ax2a supercell) in the first Brillouin zone. The details of the calculation of the isomer shift and quadrupole splitting can be found in references [29] and [30].

To check the precision of our calculations, we performed several additional calculations. In order to determine a well-justified error-bar we follow the procedure described by some of us in ref. [31]. Calculations performed using LDA and the different parameterizations of GGA predicted structural, electronic and hyperfine properties that differ in less than 2%. By examining the effect of different basis sets and k-point samplings we conclude that for the previously reported parameters relative errors are 1% or less. Based on all these studies we can infer that our results are very well converged, giving confidence to our conclusions.

4. Results and discussion

Figure 1 displays GIXRD pattern of the obtained Sn-Sb-Te film grown on mylar substrate, whose main characteristic feature is a broaden peak at nearly 26°. The Bragg peaks mounted on mylar' signal were identified as a NaCl-type structure of, nominally, $SnSb_2Te_4$ film (Fm-3m), in accordance with previous results [9]. It is worth noting that $SnSb_2Te_4$ phase adopts hexagonal R-3m space group for material in bulk or powders [32], but films prepared by pulsed laser deposition technique grow adopting cubic Fm-3m space group. The inset of Figure 1 shows the simulated XRD pattern of $SnSb_2Te_4$ phase, validating the aforementioned NaCl-type of Sn-Sb-Te film grown.

The experimental pattern presented in Figure 1 was acquired in grazing geometry (the angle of incidence $\omega = 0.3°$). No evidence of the formation of other crystalline phase was found within the threshold of the technique. It is necessary to underline that GIXRD experiments were also performed at higher incident angles in order to obtain information from the deepest layers of the film. For example, for $\omega = 1°$, one gets information approximately from the upper 90 nm of the film (for cubic $SnSb_2Te_4$). On the other hand, for $\omega = 3°$, all the film's thickness is penetrated by the x-ray beam. Again, only the crystalline Fm-3m phase was detected.

Table 1
Hyperfine parameters extracted from the fitting procedure of the ICEM spectrum: isomer shift (IS, mm/s), quadrupole splitting (QS, mm/s), area (A, %), line width (G, mm/s). Subindex is the number of the interaction.

IS_1	QS_1	A_1	G_1	IS_2	A_2	G_2
-0.01(2)	0.47(9)	85(1)	1.40(8)	3.46(3)	15(1)	0.9(2)

4.1. ICEMS

Figure 2 presents the obtained ^{119m}Sn integral conversion electron Möβbauer spectrum of the SST film. Table 1 contains all the details of the fitted parameters that characterize the ICEM spectrum. Two interactions with essentially distinct isomer shifts (IS) were identified that allows discriminating among two tin fractions: Sn(II) and Sn(IV). The hyperfine interaction characterised by the largest IS (Table 1, 2nd interaction) is attributed to Sn(II) at the sites of the NaCl-type Sn-Sb-Te structure. This interaction, due to its low intensity and lack of appreciated quadrupole splitting, was fitted to a singlet.

As it is well-known, Sn is easily oxidized in presence of oxygen [33, 34]. Its natural oxidation state is 4+ with the formulation SnO_2. The film was in a contact with air before being located into the camera (containing inert gas) for ICEMS measurements after its growth. It was discovered that tin chalcogenide systems resulted air sensitive: after 5 min exposure to air, a Sn(IV) fraction was increased twice (with respect to a Sn(II) fraction) in nanocrystals of SnS [35]. Moreover, the effect of tin oxidation in nanocrystals of SnTe was even more prominent. Interestingly, the observed Sn(IV)- containing phases were amorphous.

Most likely our film suffered oxidation during its exposure to air. This could explain the existence of Sn(IV) in the ICEMS spectrum. The only phase that might have been formed on the surface of the films with Sn (IV) and having the revealed hyperfine parameters is SnO_2 [36]. Since no footprints of crystalline SnO_2 were detected in GIXRD pattern, more likely, we deal with amorphous tin dioxide. The broad line width (1.40 mm/s) also suggests that. Interestingly, in $Ge_2Sb_2Te_5$ film the existence of amorphous Ge-O island boundaries was reported as a result of oxygen exposure [37].

To give a quantitative analysis of the tin populations (n_i), the fitted areas (A_i) have to be corrected by the corresponding value of Lamb-Möβbauer factor (the recoil-free fraction of tin atoms contributing to the Möβbauer effect), f_{LM} (f_i) as it is shown in eq.1. [38]:

$$n_i = \frac{A_i/f_i}{\sum A_i/f_i} \quad (1)$$

In its turn, the value of Lamb - Möβbauer factor can be estimated (for given temperature, T) once, when the Debye temperature, θ_D, of the phase is known [39]:

$$f = \exp\left(-\frac{6T.E_R}{k_B .\theta_D^2}\right) \quad (2)$$

where $E_R = 2.57 \times 10^{-3}$ eV is the recoil energy of the γ-ray for ^{119}Sn and k_B the Boltzmann constant. It is worth noting that eq.(2) is only an approximation and implies the Debye model in the high tempertature limit ($T \geq \theta_D$).

For amorphous SnO_2 phase, the reported f_{LM} value found in the literature is 0.4 for room temperature [39]. Using $\theta_D = 160$ K, reported for cubic $SnSb_2Te_4$ [40], the estimated f_{LM} value for cubic $SnSb_2Te_4$ at room temperature is around 0.12. Taking into account that, the areas A_i from table 1 were revised. The corrected amounts of the Sn(IV) and Sn (II) populations (n_i) in the ICEMS spectrum are roughly 60 % for Sn (IV) and 40 % for Sn (II). They differ substantially from those from table 1, but we have to remark again that these results are a rough approximation to the tin fractions and rely on the validity of the Lamb-Mössbauer factors reported in the literature. Also, it is well known that the value of these factors depends on the sample preparation method and the nature

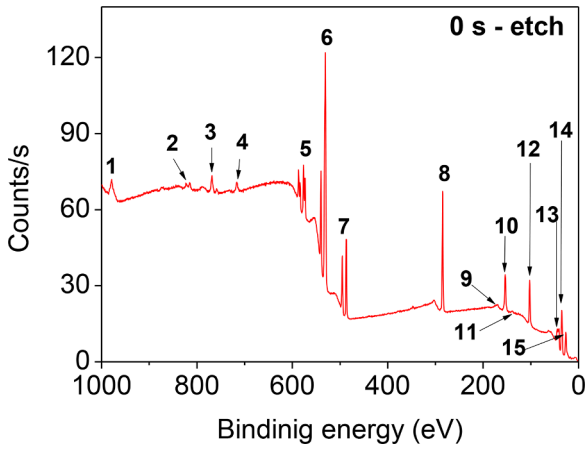

Fig. 3. Survey XP spectrum of Sn-Sb-Te film. The scale of the y-axis is reduced by 10^4 factor. 1: O KLL; 2: Te 3p; 3: Sb 3p; 4: Sn 3p; 5: Te 3d; 6: Sb 3d + O 1s; 7: Sn 3d; 8: C 1s; 9: Te 4s; 10: Sb 4s; 11: Sn 4s; 12: Sb 4p; 13: Te 4d; 14: Sb 4d; 15: Sn 4d.

of the samples (bulk samples or thin films). It is worth mentioning about the depth information that can be extracted form a ICEMS experiment. In case of tin L_1 – conversion electrons, whose energy is 19.4 keV, the mean penetration depth is estimated to be at least 1-2 μm [41]. Taking into account the thicknesses of our film, ICEMS gives its complete profile. This conclusion was checked by the following experiment: the film/mylar system was put into the camera backwards. Exactly the same profile of the spectrum was obtained, meaning that the mylar is transparent to gamma rays, and the Möβbauer information gathered was from the complete thickness of the film.

4.2. XPS

The survey XP spectrum of Sn-Sb-Te film's surface is shown in Figure 3 (where 0 corresponds to Fermi level). The well-defined peaks associated with the Sn, Sb and Te core levels were identified using the database of the Avantage software. Beyond the expected elements that constituted the film, the presence of O and C (usually found on any surface exposed to air) was clearly registered.

Figure 4A shows a high-resolution XP spectra in the range 480-500 eV binding energy (BE). Each spectrum displays the spin-orbit splitting characteristics of Sn 3d core-sublevels, namely, $3d_{5/2}$ and $3d_{3/2}$. During the deconvolution of the spectra, Sn-$3d_{5/2}$ - $3d_{3/2}$ splitting is kept 8.41 eV, in agreement with the literature [42]. In Figure 4B the spectrum of as made sample (corresponding to 0 s - etch) was deconvoluted in a pair of peaks (495.16 and 486.75 eV) assigned to Sn(IV). Each pair corresponds to a specific chemical element of the absorbing atom. A number of pairs in the fit provides a number of possible chemical environment for the absorbing atom. The area under each pair of peaks (weighed by atomic sensitivity factor if there is more than 1 chemical element under consideration) provides the concentration of the corresponding element in the sample. After the first step of sputtering (40 s) a pair of peaks with similar values of binding energies was found. Each cycle of sputtering with the selected energy removes some layers of the material. The thickness of the removed material per sputtering cycle was estimated to be at least 4.4 nm (but in fact it is more). After removing at least 9 nm - layer of the film, other pair of Sn 3d peaks appears (493.89 and 485.47 eV), besides the aforementioned ones. The latter persists up to the latest removing experience (at least, about 40 nm – layer of the film) and can be unambiguously assigned to Sn(II) in (nominally) $SnSb_2Te_4$ cubic phase. Meanwhile the signal of Sn(IV) assigned to Sn - O bonds in SnO_2, was gradually depleting after each removing cycle and was quantified at around 4 % after 360 s – sputtering.

The presence of two types of tin species found by XPS supports the information provided by ICEMS technique. At the same time this fact rises a new question: what happened with Sb and Te when tin does not form $SnSb_2Te_4$? The following figures shed light on the aforementioned concern.

Figure 4C shows a high-resolution XP spectra in the range of 525 - 544 eV BE. Each spectrum displays the spin-orbit splitting characteristics of Sb-3d core-sublevels, namely, $3d_{5/2}$ and $3d_{3/2}$. During the deconvolution of the spectra, Sb-$3d_{5/2}$ - $3d_{3/2}$ splitting is kept 9.34 eV, in agreement with the literature [42]. In Figure 4D the spectrum of as made sample (corresponds to 0 s - etch) was deconvoluted in a pair of peaks (539.83 and 530.43 eV) assigned to Sb(III) and additionally had a feature, the signal belonging to O 1s core-level (532.43 eV) in accordance with the reference [43]. As in the case of the Sn spectra, after 2 cycles of removed material, a second pair of peaks with substantially distinct BEs appeared (537.60 and 528.23 eV). The latter persists up to the latest removing and can be assigned to Sb in $SnSb_2Te_4$ structure, meanwhile the pair of 3d peaks with higher binding energy is attributed to Sb-O bond in likely Sb_2O_3 [44]. As in the case of tin oxide, the presence of antimony oxide was registered in all the expected layers with similar depleting trend being quantified close to 4 % after the last removing. Antimony oxidation was also reported in $Ge_2Sb_2Te_5$ films [18].

The spectra shown in Figure 4E in the range of 567-590 eV BE display Te-3d core-level. During the deconvolution of the spectra, Te-$3d_{5/2}$ - $3d_{3/2}$ splitting is kept 10.39 eV, in agreement with the literature [42]. Unlike the spectra of Sn and Sb, the Te spectrum corresponding to the case of 0 s – etch was fitted to two pair of peaks (Figure 4F). One pair of peaks with values of 586.74 and 576.37 eV was assigned to Te-$3d_{3/2}$ and $3d_{5/2}$, respectively, of Te - O bonds in likely TeO_2. The second pair of peaks of 0 s - sputtering spectrum was 583.58 and 573.21 eV. Wu et al. in their study of $SnSb_2Te_4$ (R-3m space group) assigned the doublet with very similar BE to Te-C bond [13]. We cannot discard it in our case since the surface of the film was rich in carbon. It is worth noting, after 40 s – sputtering and therinafter, TeO_2 (unlike SnO_2 and Sb_2O_3) was absent. After 80 s – sputtering a signal with slightly distinct (0.7 eV lower) set of BE is born. It means Te is forming a bond with a less electronegative element (like Sn or/and Sb in our case). This signal is attributed to Te in $SnSb_2Te_4$. Hereinafter, the BE are 582.9 and 572.5 eV until the last sputtering cycle.

Formation of oxides on surfaces is a frequent situation for chalcogenide – containing systems exposed to air and was found in a number, in particular, of Te-containing systems: SnTe, Sb_2Te_3, $SnSb_2Te_4$, $Ge_2Sb_2Te_5$, etc. Based on the XP spectra as a function of sputtering time it was possible to follow the in-depth atomic concentration profiles in the film (Table 2). The general trend is the lacking of the expected stoichiometry: a deficient Te presence is notoriuos. In particular, the top layers of the Sn-Sb-Te film are rich in antimony and poor in tellurium. Approximately after at least 9-10 nm inside the film, the atomic profile of the cubic Sn-Sb-Te specie is kept practically unchanged (averaged, $Sn_{25}Sb_{32}Te_{43}$) in the inspected region but deflecting notoriously from the nominal stoichiometry. For instance, it is well known about Te volatility during the growing process of the films. This could explain the lower tellurium content in the sample. Interestingly, in spite of the lack of stoichiometry seen by XPS, the GIXRD pattern was clearly compatible with cubic $SnSb_2Te_4$. The possible explanation is Te - poor sites of nominally $SnSb_2Te_4$ phase's layers were substituted with O as a result of exposure to air as it was suggested in ref.[18] for $Ge_2Sb_2Te_5$. This hypothesis has been explored by means of comparing the experimentally obtained results with those predcited by the DFT calculations assuming different scenarios.

4.3. DFT-study

The analysis of the Möβbauer spectrum of $SnSb_2Te_4$ films provides an evidence of two interactions, each one with different hyperfine parameters. These interactions were associated with Sn(II) in the NaCl-

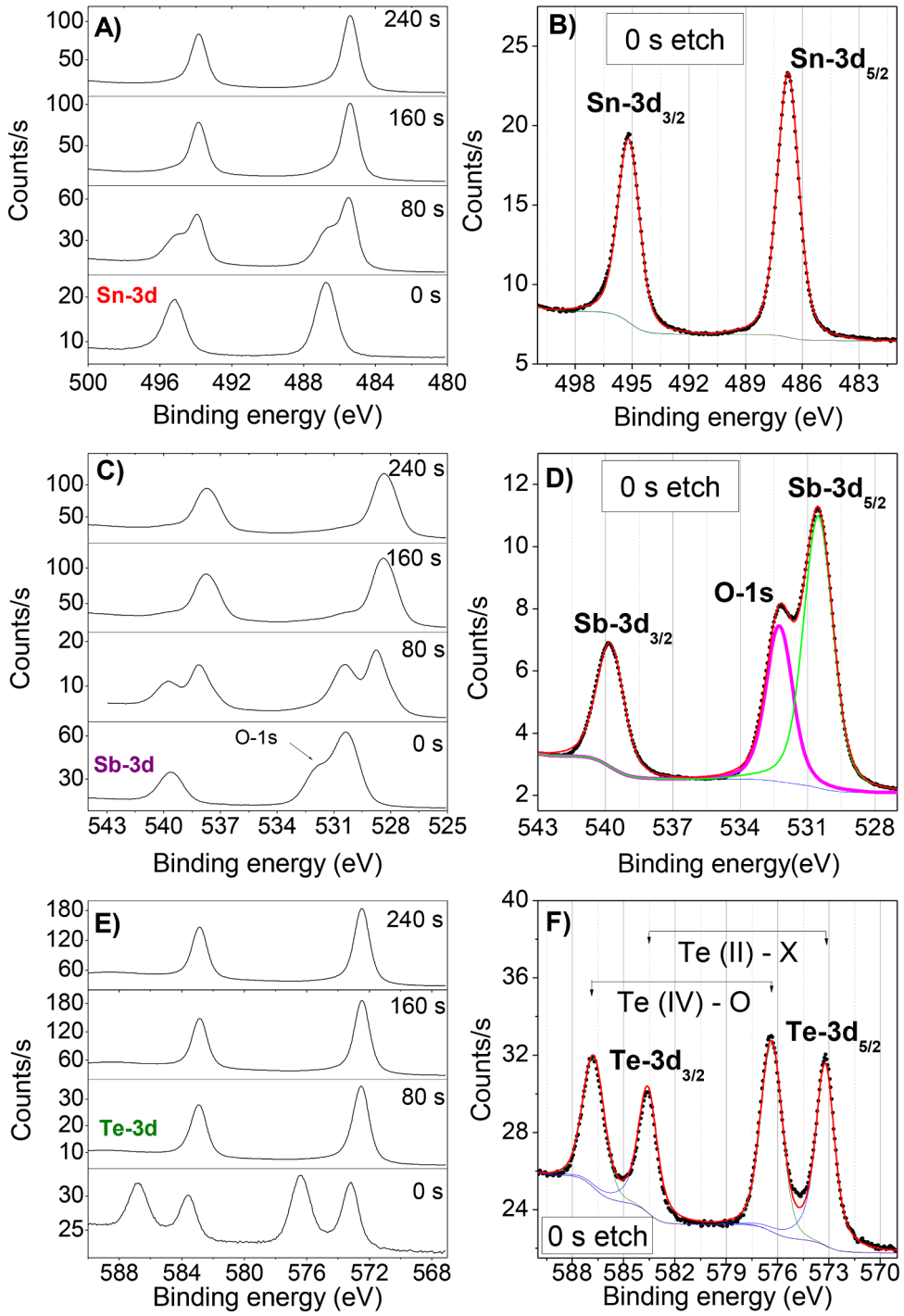

Fig. 4. The evolution of 3d core-level spectra of A) Sn; C) Sb; E) Te as a function of etch time. After each sputtering cycle (40 s) the XPS depth profiling analysis has been done (only selected spectra are shown). The deconvolution of 0 s - etch spectra of B) Sn; D) Sb and F) Te are also shown. The scale of all the y-axis is reduced by 10^4 factor.

structure of Sn-Sb-Te film, and also with Sn(IV) attributed to the presence of tin dioxide likely in an amorphous state. To support this interpretation of the observed hyperfine interactions we performed density-theory based ab initio calculations. For this purpose, we determined the self-consistent potential and the charge density of the $SnSb_2Te_4$ host and then the quadrupole splitting and the isomer shift at the Sn probe nucleus replacing Sb atoms and considering the presence of Sb vacancies and oxygen atoms.

As it was mentioned before, $SnSb_2Te_4$ film crystallizes in the cubic NaCl-type structure, being isostructural with $GeSb_2Te_4$ [45], Fm-3m space group. One sublattice is occupied by Te atoms, the other sublattice by Sb (50%), Sn (25%) and vacancy (25%). The Te and Sb atoms are located at positions (0, 0, 0) F.C. and (0.5, 0, 0) F.C., respectively. F. C. denotes that the positions can be repeated adding (0.5, 0.5, 0), (0, 0.5, 0.5) and (0.5, 0, 0.5). Initially, we removed the F.C. symmetry and performed calculations in the unit cell consisting of 8 atoms. In this cell we performed calculations replacing one Sb atom by a Sn. The substitution of one Te atom by a Sn one was also considered. The vacancy was simulated by simple removing one Sb or Te atom.

In a second step, and to better simulate the real situation we built a

Table 2
Estimated (roughly) in-depth atomic concentration profile of nominally $SnSb_2Te_4$ film. 0 nm- depth corresponds to the surface of the approximately 150 nm-thickness film.

Depth (nm)	Te (at.%)	Sb (at.%)	Sn (at.%)
39.6	40	34	26
35.2	44	33	24
30.8	43	32	25
26.4	43	32	25
22	43	32	25
17.6	43	33	24
13.2	44	33	23
8.8	45	35	20
4.4	29	41	30
0	25	46	29

64-atom supercell with the dimensions 2a × 2a × 2a. The Sn and vacancy-concentrations have been simulated replacing eight Sb-atoms by Sn ones and removing eight Sb atoms (for these calculations, based on the results obtained for the unit cell, we only considered the case of Sn and vacancies located in the Sb-sublattice). Here a situation appears that has to be solved: the distribution of 8 Sn atoms and 8 vacancies in the 32 Sb sites of the supercell. To deal with this problem, we performed calculations for different distributions of the Sn and Sb-vacancies in these 32 sites taking into account the changes in the volume cell and the internal structural distortions induced by the tin atoms and the vacancies

As the first step we performed calculations using the unit cell for the study of the localization of the Sn atoms in the structure and to confirm that the vacancies are formed in the Sb sublattice. For this purpose, we studied four cases:

$SnSb_2Te_4$ (Sn replacing Sb, one Sb vacancy)
$SnSb_3Te_3$ (Sn replacing Sb, one Te vacancy)
Sb_2SnTe_3 (Sn replacing Te, one Sb vacancy)
Sb_3SnTe_2 (Sn replacing Te, one Te vacancy)

To estimate the stable structure, we compared the formation energy of each system, E^{form}, defined as:

$$E^{form} = E - \sum_i n_i E_i^{at} \quad (3)$$

Here E is the total energy of the unit-cell containing a single substitutional Sn atom and a Sb or Te vacancy, E_i^{at} denotes the energy of the Te, Sb and Sn atoms, and n_i the number of Sn, Te, and Sn atoms in the unit cell in each case. The formation energies were obtained by calculating the energies of each of the four systems considered and E_i^{at} from metallic Sn, Sb, and Te with the same precision as that in the Sn-Sb-Te compounds. The obtained results were:

$E^{form}(SnSb_2Te_4) = -15.9$ eV
$E^{form}(SnSb_3Te_3) = -14.4$ eV
$E^{form}(Sb_2SnTe_3) = -15.3$ eV
$E^{form}(Sb_3SnTe_3) = -11.4$ eV

It means the system $SnSb_2Te_4$ (Sn replacing Sb and a vacancy in the Sb sublattice) is the most stable one. For this system, we obtained that the equilibrium lattice parameter is 6.12 Å, slightly smaller than the experimental one, 6.19 Å [9]. This underestimation of the lattice parameter can be attributed to the small size of the cell used for the calculation of the system with tin and Sb-vacancies. $SnSb_2Te_4$ presents a metallic nature and the hyperfine parameters at the Sn sites are IS = 3.20 mm/s, QS = 0.28 mm/s.

For this cell we also evaluated the effect on the hyperfine parameters of the presence of an oxygen atom. When an oxygen atom replaces a Te atom located in the first coordination shell of Sn, the IS grows to 3.40 mm/s. This value is very close to the experimental one, 3.46 mm/s. We also considered the possibility of an interstitial oxygen atom. For this case, IS = 3.10 mm/s, moving away from the experimental result.

After that, we extend our study to the 2ax2ax2a supercell. As it was

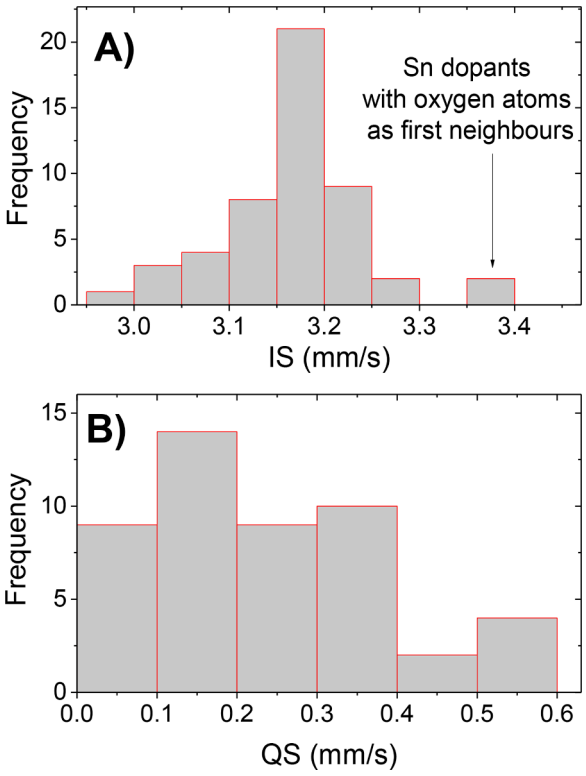

Fig. 5. Isimer shift (left) and quadrupole splitting (right) results obtained at each Sn site for all the configurations considered. The results correspond to the ab initio calculations performed in the 2ax2ax2a supercell and considering that tin atoms subtitute Sb atoms in the Te-Sb structure and considering vanacies at the Sb sites.

aforementioned, we have to solve the problem of the distribution of the Sn atoms in the structural sites of the Te-Sb cell. Based on the results obtained for the case of the unit cell and the experimental result, we focus on the case of Sn and vacancies in the Sb-sublattice. So, we have to determine the distribution of 16 Sb atoms, 8 Sn and 8 Sb vacancies at the 32 Sb sites. Initially, we replace two Sb atoms by Sn ones, and we study the energy of the system as a function of the Sn-Sn separation. We obtained that the energy of the system is irrespective of the localization of the Sn dopants. A similar result was obtained for the case of only two Sb-vacancies. Finally, we considered the case of one Sn and one Sb vacancy. Again, the energy of the system is nearly independent of the Sn-Sb-vacancy site separation. After that and based on all these results we performed calculations considering different random distributions of Sn and Sb-vacancies in the Sb sublattice. We obtained that the energy difference between the configurations is relatively small, suggesting that the overall properties of the Sn-Sb-Te sample are a statistical average of different Sn-Sb vacancies configurations and the experimental results must be compared only with these average estimations.

For all these configurations we obtained that the equilibrium lattice parameter is 6.15 Å. This result is nearly irrespective of the configuration considered (differences smaller than ± 0.02 Å). The results for the IS and the QS are presented in Figure 5. The average IS is 3.17 mm/s and is characterised by a narrow distribution, showing that the IS is nearly independent of the Sn and vacancies distribution. In the case of the QS, the average value is 0.22 mm/s with a standard deviation of 0.15 mm/s. This distribution in the QS value is expected due to the extreme sensitivity of the QS to small changes in the asymmetry of the charge density in the close vicinity of the Sn probe. Note that these average values for the IS and the QS are similar to those obtained in the case of the calculations performed considering the unit cell with one Sn and one Sb vacancy. When an oxygen vacancy is included in the calculations, the tin

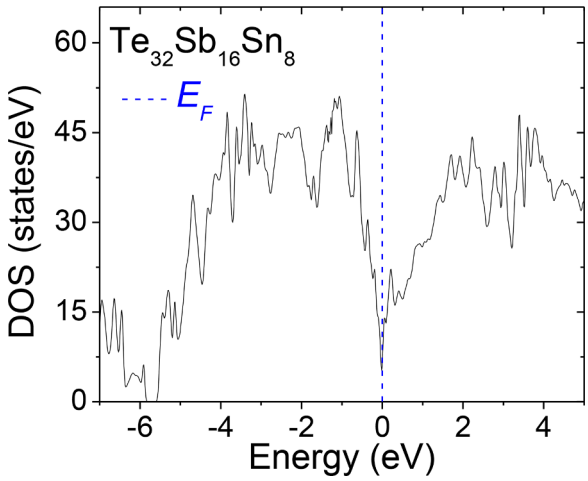

Fig. 6. Total density of states (DOS) of Te-Sb-Sn. Energies are referred to the Fermi level (E_F, 0.0 eV).

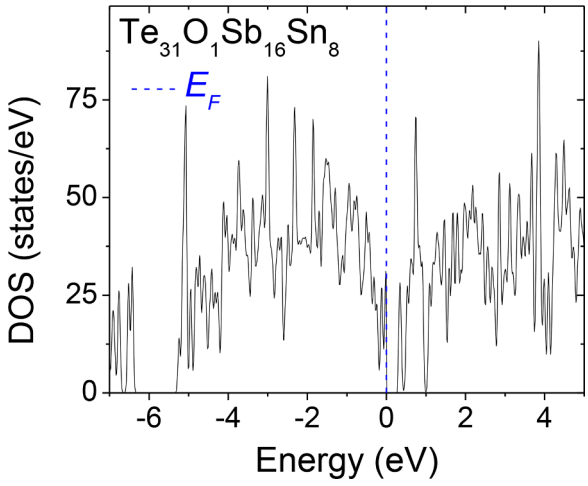

Fig. 7. Total density of states (DOS) of Te-Sb-Sn.with oxygen vacancies at the Te sites. Energies are referred to the Fermi level (E_F, 0.0 eV).

atoms that have (at least) one oxygen at a first-neighbour Te-site present an IS in the order of 3.35 mm/s. Also, when oxygen atoms are incorporated, the system becomes semiconductor with a band-gap in the order of 0.3 eV (Figure 6 and 7). These results confirm that the experimentally observed hyperfine interaction characterized by an IS of 3.47 mm/s is related with the oxidation of the sample. As it can be seen these results support the hypothesis we put forward about the formatin of Te vacancies that are occupied by O atom in the sample.

5. Conclusions

By means of surface sensitive techniques such as GIXRD, ICEMS and XPS, the structural study and chemical analysis of nominally $SnSb_2Te_4$ thin film grown on mylar by pulsed laser deposition were performed. GIXRD showed that the grown film was polycrystalline and adopts a NaCl-type crystalline structure. ^{119m}Sn ICEMS demonstrated the presence of two tin environments: the expected Sn(II) located at the sites of the NaCl – type Sn-Sb-Te film, and also a fraction of Sn(IV) that was attributed to the presence of tin dioxide, likely, in an amorphous state. It has been found by XPS that uncapped $SnSb_2Te_4$ film is prone to oxidation and that the topmost layers (at least about 10 nm tickness) of the studied film exposed to oxygen become depleted of Te and transformed into Sn-O, Sb-O and Te-O. Underneath approximately 10 nm and down to, at least, 40-50 nm, the sample is mostly Sn-Sb-Te crystalline phase keeping the inalterable distribution of the elements albeit with deviation from the stoichiometric $SnSb_2Te_4$ with a notorious lacking of Te. DFT-based calculations performed considering $SnSb_2Te_4$ with the Fm-3m structure showed that this system presents a metallic nature and only with oxygens substitutionally located at Te-vacancy sites the system presents a semiconducting behaviour with a band gap of about 0.3 eV. The isomer shift at Sn sites with O atoms in their first coordination shell for the aforementioned case is in excellent agreement with those experimentally found in the film affected by the oxidation process.

CRediT authorship contribution statement

V. Bilovol: Project administration, Investigation, Conceptualization, Methodology, Validation, Writing – original draft, Writing – review & editing, Supervision. **H.H. Medina Chanduví:** Software, Methodology, Writing – review & editing. **L.A. Errico:** Conceptualization, Methodology, Writing – review & editing, Validation.

Declaration of Competing Interest

The authors declare that they have no known competing financial interests or personal relationships that could have appeared to influence the work reported in this paper.

Acknowledgements

We want to thank Dr. B. Arcondo for fruitful discussions. This work was partially supported by the Universidad de Buenos Aires (UBACyT 20020190200037BA). The research was also partially supported by the CONICET (grant no. PIP 0039-2017) and UNLP (grants no. 11/X845 and X806/18).

References

[1] Y. Yu, M. Cagnoni, O. Cojocaru-Mirédin, M. Wuttig, Chalcogenide Thermoelectrics Empowered by an Unconventional Bonding Mechanism, Adv. Funct. Mater. 30 (2020), 1904862, https://doi.org/10.1002/adfm.201904862.
[2] B.J. Kooi, M. Wuttig, Chalcogenides by Design: Functionality through Metavalent Bonding and Confinement, Adv. Mater. 32 (2020), 1908302, https://doi.org/10.1002/adma.201908302.
[3] P. Guo, A.M. Sarangan, I. Agha, A Review of Germanium-Antimony-Telluride Phase Change Materials for Non-Volatile Memories and Optical Modulators, Appl. Sci. 9 (2019) 530, https://doi.org/10.3390/app9030530.
[4] Y. Ando, Topological Insulator Materials, J. Phys. Soc. Jpn. 82 (2013), 102001, https://doi.org/10.7566/JPSJ.82.102001.
[5] Jian-Feng Ge, Zhi-Long Liu, Canhua Liu, Chun-Lei Gao, Dong Qian, Qi-Kun Xue, Ying Liu, Jin-Feng Jia, Superconductivity above 100 K in single-layer FeSe films on doped SrTiO3, Nat. Mater. 14 (2015) 285–289, https://doi.org/10.1038/nmat4153.
[6] G.Bakan B.Gerislioglu, J.Adam R.Ahuja, A.Ahmadivand Y.K.Mishra, The role of Ge2Sb2Te5 in enhancing the performance of functional plasmonic devices, Mater. Today Phys. 12 (2020) 10078, https://doi.org/10.1016/j.mtphys.2020.100178.
[7] Il-Mok Park, Jung-Kyu Jung, Sang-Ouk Ryu, Kyu-Jeong Choi, Byoung-Gon Yu, Park Seung Min Han Young-Ba, Young-Chang Joo, Thermomechanical properties and mechanical stresses of Ge2Sb2Te5 films in phase-change random access memory, Thin Solid Films 517 (2008) 848–852, https://doi.org/10.1016/j.tsf.2008.08.194.
[8] J. Lee, T. Kodama, Y. Won, M. Asheghi, K.E. Goodson, Phase purity and the thermoelectric properties of Ge2Sb2Te5 films down to 25 nm thickness, J. Appl. Phys. 112 (2012), 014902, https://doi.org/10.1063/1.4731252.
[9] V. Bilovol, B. Arcondo, J.A. Rocca, E.J. Di Liscia, M.A. Ureña, SnSb2Te4: Microcrystalline sample vs thin film, J. Solid State Chem. 285 (2020), 121249, https://doi.org/10.1016/j.jssc.2020.121249.
[10] J. Reindl, H. Volker, N.P. Breznay, M. Wuttig, Persistence of spin memory in a crystalline, insulating phase-change material, Quantum Mater. 4 (2019) 57, https://doi.org/10.1038/s41535-019-0196-6.
[11] P. Song, R. Matsumoto, Zh. Hou, Sh. Adachi, H. Hara, Y. Saito, P.B. Castro, H. Takeya, Y. Takano, Pressure-induced superconductivity in $SnSb_2Te_4$, J, Phys.: Condens. Matter. 32 (2020), 235901, https://doi.org/10.1088/1361-648X/ab76e2.
[12] J.A. Sans, R. Vilaplana, E. Lora da Silva, C. Popescu, V.P. Cuenca-Gotor, A. Andrada-Chacón, J. Sánchez-Benitez, O. Gomis, A.L.J. Pereira, P. Rodríguez-Hernández, A. Muñoz, D. Daisenberger, B. García-Domene, A. Segura, D. Errandonea, R.S. Kumar, O. Oeckler, Ph. Urban, J. Contreras-García, F. J. Manjón, Characterization and Decomposition of the Natural van der Waals

SnSb2Te4 under Compression, Inorg. Chem. 59 14 (2020) 9900–9918, https://doi.org/10.1021/acs.inorgchem.0c01086.
[13] Zh. Wu, G. Liang, W.K. Pang, T. Zhou, Zh. Cheng, W. Zhang, Ye Liu, B. Johannessen, Z. Guo, Coupling Topological Insulator SnSb2Te4 Nanodots with Highly Doped Graphene for High-Rate Energy Storage, Adv. Mater. 32 (2020), 1905632, https://doi.org/10.1002/adma.201905632.
[14] X. Zhou, M. Xia, F. Rao, L. Wu, X. Li, Z. Song, S. Feng, H. Sun, Understanding phasechange behaviors of carbon-doped Ge2Sb2Te5 for phase-change memory application, ACS Appl. Mater. Interfaces 6 (2014) 14207, https://doi.org/10.1021/am503502q.
[15] K.H. Kim, J.G. Chung, Y.K. Kyoung, J.C. Park, S.J. Choi, Phase-change characteristics of nitrogen-doped Ge2Sb2Te5 films during annealing process, J. Mater. Sci.: Mater. Electron. 22 (2011) 52–55, https://doi.org/10.1007/s10854-010-0081-3.
[16] T.H. Jeong, H. Seo, K.L. Lee, S.M. Choi, S.J. Kim, S.Y. Kim, Study of oxygen-doped GeSbTe film and its effect as an interface layer on the recording properties in the blue wavelength, Jpn J. Appl. Phys. 40 (2001) 1609, https://doi.org/10.1143/JJAP.40.1609.
[17] R. Berthier, N. Bernier, D. Cooper, C. Sabbione, F. Hippert, P. Noé, In situ observation of the impact of surface oxidation on the crystallization mechanism of GeTe phase-change thin films by scanning transmission electron microscopy, J. Appl. Phys. 122 (2017), 115304, https://doi.org/10.1063/1.5002637.
[18] R. Golovchak, Y.G. Choi, S. Kozyukhin, Yu. Chigirinsky, A. Kovalskiy, P. Xiong-Skiba, J. Trimble, H.Jain R.Pafchek, Oxygen incorporation into GST phase-change memory matrix, Appl. Surf. Sci. 332 (2015) 533–541, https://doi.org/10.1016/j.apsusc.2015.01.203, https://doi.org/.
[19] M. Agati, C. Gaya, D. Benoit, A. Claverie, Effects of surface oxidation on the crystallization characteristics of Ge-rich Ge-Sb-Te alloys thin films, Appl. Surf. Sci. 518 (2020), 146227, https://doi.org/10.1016/j.apsusc.2020.146227.
[20] R.A. Brand, Normos Programs (SITE-DIST), Duisburg University, 1991.
[21] P. Blaha, K. Schwarz, G. Madsen, D. Kvasnicka, J. Luitz, R. Laskowski, F. Tran, L. Marks, WIEN2k, An Augmented Plane Wave þ Local Orbitals Program for Calculating Crystal Properties, Karlheinz Schwarz, Techn, Universitt Wien, Austria, 2018. ISBN 3-9501031-1-2.
[22] E. Sjöstedt, L. Nordström, D.J. Singh, An Alternative Way of Linearizing the Augmented Plane-Wave Method, Solid State Commun. 114 (2000) 15–20, https://doi.org/10.1016/s0038-1098(99)00577-3.
[23] G.K.H. Madsen, P. Blaha, K. Schwarz, E. Sjöstedt, L. Nordström, Efficient Linearization of the Augmented Plane-Wave Method, Phys. Rev. B 64 (2001), 195134, https://doi.org/10.1103/PhysRevB.64.195134.
[24] S. Cottenier, Density Functional Theory and the Family of (L)APW-Methods: A Step-by-Step Introduction, KU Leuven, Belgium, 2002. http://www.wien2k.at/reg_user/textbooks.
[25] J.P. Perdew, Y. Wang, Accurate and simple analytic representation of the electron-gas correlation energy, Phys. Rev. B 45 (1992) 13244, https://doi.org/10.1103/physrevb.45.13244.
[26] Z. Wu, R.E. Cohen, More accurate generalized gradient approximation for solids, Phys. Rev. B 73 (2006), 235116, https://doi.org/10.1103/PhysRevB.73.235116.
[27] J.P. Perdew, K. Burke, M. Ernzerhof, Generalized gradient approximation made simple, Phys. Rev. Lett. 7 (1996) 3865–3868, https://doi.org/10.1103/physrevlett.77.3865.
[28] J.P. Perdew, A. Ruzsinszky, G.I. Csonka, O.A. Vydrov, G.E. Scuseria, L. A. Constantin, X. Zhou, K. Burke, Restoring the Density-Gradient Expansion for Exchange in Solids and Surfaces, Phys. Rev. Lett. 100 (2008), 136406, https://doi.org/10.1103/PhysRevLett.100.136406.
[29] A.V. Gil Rebaza, L.A. Errico, E.L. Peltzer y Blancá, A.M. Mudarra Navarro, DFT-based study of the structural, electronic and hyperfine properties of the semiconducting alloys $Sn_{1-x}Ti_xO2$: HSE06 and non-regular TB-mBJ approach, Mater. Chem. Phys. 237 (2019), 121874, https://doi.org/10.1016/j.matchemphys.2019.121874.
[30] H.H. Medina Chanduví, A.M. Mudarra Navarro, V. Bilovol, L.A. Errico, A.V. Gil Rebaza, Structural, Electronic, Magnetic, and Hyperfine Properties of V-doped SnO_2 ($Sn_{1-x}V_xO_2$, x: 0, 0.042, 0.084, and 0.125). A DFT-Based Study, J. Phys. Chem. C 125 (2021) 11702–11713, https://doi.org/10.1021/acs.jpcc.1c02285.
[31] L.A. Errico, K. Lejaeghere, J. Runco, S.N. Mishra, M. Rentería, S. Cottenier, Precision of Electric-Field Gradient Predictions by Density Functional Theory and Implications for the Nuclear Quadrupole Moment and Its Error Bar of the ^{111}Cd 245 keV 5/2+ Level, J. Phys. Chem. C 120 (2016) 23111–23120.
[32] T. Schafer, Ph M. Konze, J.D. Huyeng, V.L. Deringer, Th. Lesieur, P. Müller, M. Morgenstern, R. Dronskowski, M. Wuttig, Chemical tuning of carrier type and concentration in a homologous series of crystalline chalcogenides, Chem. Mater. 29 (2017) 6749–6757, https://doi.org/10.1021/acs.chemmater.7b01595.
[33] S. Cho, J. Yu, S.K. Kang, Da-Y. Shih, Oxidation study of pure tin and its alloys via electrochemical reduction analysis, J. Electron. Mater. 34 (2005) 635–642, https://doi.org/10.1007/s11664-005-0077-6.
[34] Y.-H. Wang, M.R Howlader, K. Nishida, T. Kimura, T. Suga, Study on Sn–Ag Oxidation and Feasibility of Room Temperature Bonding of Sn–Ag–Cu Solder, Mater. Trans. 46 (2005) 2431–2436.
[35] A. de Kergommeaux, J. Faure-Vincent, A. Pron, R. de Bettignies, B. Malaman, P. Reiss, Surface Oxidation of Tin Chalcogenide Nanocrystals Revealed by ^{119}Sn-Mössbauer Spectroscopy, J. Am. Chem. Soc. 134 (2012) 11659–11666, https://doi.org/10.1021/ja3033313.
[36] S. Yu. Vassiliev, A.I. Yusipovich, Yu.E. Rogynskaya, F. Kh. Chibirova, A. M. Skundin, T.L. Kulova, Nanostructured SnO_2-TiO_2 films as related to lithium intercalation, J. Solid State Electrochem. 9 (2005) 698–705, https://doi.org/10.1007/s10008-005-0646-x.
[37] S. Tripathi, P. Kotula, M. Singh, C. Ghosh, G. Bakan, H. Silva, C.Barry Carter, Role of Oxygen on Chemical Segregation in Uncapped Ge2Sb2Te5 Thin Films on Silicon Nitride, J. Solid State Sci. Technol. 9 (2020), 054007, https://doi.org/10.1149/2162-8777/ab9a19.
[38] F. Robert, F. Morato, J. Chouvin, L. Aldon, P.E. Lippens, J.O. Fourcade, J.-C. Jumas, B. Simon, Ph. Biensan, Structural and electronic modifications induced by lithium insertion in Sn-based oxide glasses, J. Power Sources 119–121 (2003) 581–584, https://doi.org/10.1016/S0378-7753(03)00294-5.
[39] M.T. Sougrati, S. Jouen, B. Hannoyer, Relative Lamb–Mössbauer factors of tin corrosion products, Hyperfine Interact. 167 (2006) 815–818, https://doi.org/10.1007/s10751-006-9363-9.
[40] J. Gallus, Lattice Dynamics in the SnSb2Te4 Phase Change Material, Diplomarbeit in Physik, Fakultät für Mathematik, Informatik und Naturwissenschaften der Rheinisch-Westfalischen Technischen Hochschule Aachen, 2011. http://hdl.handle.net/2128/23285.
[41] K. Nomura, Y. Ujihira, E. Kuzmann, K. Kurosawa, Characterization of tin coated Al alloy by ^{119}Sn conversion electron Mössbauer spectrometry (CEMS), J. Radioanal. Nucl. Chem. 257 (2003) 97–103.
[42] J.F. Moulder, W.F. Stickle, P.E. Sobol, K.D. Bomben, Handbook of X-ray Photoelectron Spectroscopy, Perkin-Elmer Corp, Eden Prairie, MN, 1992.
[43] G. Beamson, D. Briggs, High Resolution XPS of Organic Polymers - The Scienta ESCA300 Database, Wiley Interscience, 1992. Appendices 3.1 and 3.2.
[44] C.D. Wagner, A.V. Naumkin, A. Kraut-Vass, J.W. Allison, C.J. Powell, J.R.Jr. Rumble, NIST Standard Reference Database 20, Version 3.4 (web version) (http:/srdata.nist.gov/xps/) 2003.
[45] amd T. Matsunaga, N. Yamada, Structural investigation of GeSb2Te4: A high-speed phase-change material, Phys. Rev. B 69 (2004), 104111, https://doi.org/10.1103/PhysRevB.69.104111.